International Journal of Nanomedicine

Dovepress
open access to scientific and medical research

Open Access Full Text Article

ORIGINAL RESEARCH

Design, physicochemical characterization, and optimization of organic solution advanced spray-dried inhalable dipalmitoylphosphatidylcholine (DPPC) and dipalmitoylphosphatidylethanolamine poly(ethylene glycol) (DPPE-PEG) microparticles and nanoparticles for targeted respiratory nanomedicine delivery as dry powder inhalation aerosols

This article was published in the following Dove Press journal:
International Journal of Nanomedicine
15 January 2013
Number of times this article has been viewed

Samantha A Meenach[1,2]
Frederick G Vogt[3]
Kimberly W Anderson[2,4]
J Zach Hilt[2,4]
Ronald C McGarry[5]
Heidi M Mansour[1,4]

[1]Department of Pharmaceutical Sciences-Drug Development Division, University of Kentucky College of Pharmacy, Lexington, KY; [2]Department of Chemical and Materials Engineering, University of Kentucky, Lexington, KY, USA; [3]Analytical Sciences, Product Development, GlaxoSmithKline, King of Prussia, PA; [4]Center of Membrane Sciences, University of Kentucky, Lexington, KY, [5]Department of Radiation Medicine, University of Kentucky College of Medicine, Lexington, KY, USA

Correspondence: Heidi M Mansour
Department of Pharmaceutical Sciences-Drug Development Division, University of Kentucky College of Pharmacy,
Tel +1 859 257 1571
Fax +1 859 257 7564
Email heidi.mansour@uky.edu

Abstract: Novel advanced spray-dried and co-spray-dried inhalable lung surfactant-mimic phospholipid and poly(ethylene glycol) (PEG)ylated lipopolymers as microparticulate/nanoparticulate dry powders of biodegradable biocompatible lipopolymers were rationally formulated via an organic solution advanced spray-drying process in closed mode using various phospholipid formulations and rationally chosen spray-drying pump rates. Ratios of dipalmitoylphosphatidylcholine (DPPC) and dipalmitoylphosphatidylethanolamine PEG (DPPE-PEG) with varying PEG lengths were mixed in a dilute methanol solution. Scanning electron microscopy images showed the smooth, spherical particle morphology of the inhalable particles. The size of the particles was statistically analyzed using the scanning electron micrographs and SigmaScan® software and were determined to be 600 nm to 1.2 µm in diameter, which is optimal for deep-lung alveolar penetration. Differential scanning calorimetry (DSC) and powder X-ray diffraction (PXRD) were performed to analyze solid-state transitions and long-range molecular order, respectively, and allowed for the confirmation of the presence of phospholipid bilayers in the solid state of the particles. The residual water content of the particles was very low, as quantified analytically via Karl Fischer titration. The composition of the particles was confirmed using attenuated total-reflectance Fourier-transform infrared (ATR-FTIR) spectroscopy and confocal Raman microscopy (CRM), and chemical imaging confirmed the chemical homogeneity of the particles. The dry powder aerosol dispersion properties were evaluated using the Next Generation Impactor™ (NGI™) coupled with the HandiHaler® dry powder inhaler device, where the mass median aerodynamic diameter from 2.6 to 4.3 µm with excellent aerosol dispersion performance, as exemplified by high values of emitted dose, fine particle fraction, and respirable fraction. Overall, it was determined that the pump rates defined in the spray-drying process had a significant effect on the solid-state particle properties and that a higher pump rate produced the most optimal system. Advanced dry powder inhalers of inhalable lipopolymers for targeted dry powder inhalation delivery were successfully achieved.

Keywords: biocompatible biodegradable lipopolymers, lung surfactant, pulmonary delivery, self-assemblies, solid-state, lipospheres

Introduction

The lung is an ideal target for targeted drug delivery, due to the potential to deliver therapeutic aerosols, which allows for uniform drug distribution, the avoidance of first-pass metabolism, a rapid onset of action, and high drug concentrations within the lung.[1–4] Furthermore, the presence of drug at the site of pathology with minimal systemic absorption leads to decreased side effects.[5] Inhalation aerosols enable therapeutic effects to be achieved at much lower drug doses compared to other routes of administration offering inherently longer residence time in the lungs, which can reduce dosing frequency and increase patient compliance.[2,5–8] Aerosol formulations have been investigated for many pulmonary diseases including cystic fibrosis, asthma, chronic obstructive pulmonary disease, lung infections, and lung cancer.[9–15] Inhalation aerosols for the treatment of pulmonary diseases date back to ancient times[7,16] and many inhalation products exist, of which dry powder inhalers (DPIs) are the fastest-growing segment. DPI formulations offer many advantages, including storing the drug in a dry state, leading to long-term stability,[17] the ability to encapsulate various types of therapeutics,[18] and the ease of DPI implementation.[6,19]

Dry powder aerosol formulations of nanoparticles and microparticles are of significant interest for direct lung delivery.[14,20,21] In particular, the use of phospholipids as multifunctional biocompatible biodegradable excipients for the delivery of therapeutics to the lungs is an attractive option.[22] Phospholipids have been shown to improve particle migration to the lung periphery, owing to the reduction in surface tension provided by these biosurfactants,[23–27] especially to poorly water-soluble drugs. The use of phospholipids in pulmonary delivery is logical in that lung surfactant is a mixture primarily comprised of phospholipids and smaller amounts of lung surfactant-specific surface-active proteins. In particular, dipalmitoylphosphatidylcholine (DPPC) is the primary phospholipid component in lung surfactant, making up 55%–60% of the mixture. DPPC serves a vital role in reducing the work of breathing, and pulmonary immunity modulation, and is used in several successful lung surfactant replacement nanopharmaceutical products.[14] In addition to DPPC being an innate component of the lung, it offers advantages in drug delivery owing to its transition temperature. Transition temperatures of phospholipids are highly dependent on the saturation and length of carbon chains and DPPC (a diacyl 16-saturated carbon chain phospholipid) has a transition temperature of 41°C (above physiological body temperature of 37°C) when fully hydrated, which may offer controlled drug release.[1,14,28]

The use of poly(ethylene glycol) (PEG)-based liposomal formulations has been motivated by the advantage of having biocompatible self-assembled drug-delivery systems that can evade the recognition and uptake by cells in the immune system while prolonging the residence time of the liposomes and providing sustained drug release.[14,29–32] In addition, PEG has been recently demonstrated to have inherent mucus-penetrating properties.[33] Unlike other types of inhaled particles, the fate of phospholipid-based particles can have a similar fate to native lipids. The processing, uptake, and recycling of phospholipid particles occurs through the same mechanism as endogenous surfactant via alveolar type II pneumocytes.[29] In addition, there are successful nanopharmaceutical products containing PEGylated phospholipid for intravenous administration, as it is an FDA-approved excipient.[14,20,21,32] Sterically stabilized nanomicelles comprised of PEGylated phospholipids with encapsulated drug for the treatment of acute lung injury by the intravenous route have been reported.[34,35]

The spray-drying method is an advanced high-throughput pharmaceutical manufacturing process that is used to efficiently produce and tailor respirable particles in the solid state.[2,8,14,36] Spray-drying has been used in the microencapsulation of bioactive molecules, as well as in the preparation of drug-delivery systems composed of a large variety of biodegradable polymers and excipients.[37–39] It has also been used as a scalable method in the bulk preparation of drug–lipid mixtures.[37,40,41] The unique features and tunable parameters of spray-drying allow for the precise tuning of the particle properties as a result of rational design and engineering. The use of an organic solvent allows for much lower moisture content and smaller particle size (down to 400 nm). This along with the inherently lower surface tension of the solvent combined with dilute solution concentrations allows particle formulation in the solid state in the inhalable range.

The rational design and development of inhalable lung surfactant-mimic DPPC and PEGylated phospholipid with varying PEG chain length as respirable microparticles and nanoparticles as one-component spray-dried (SD) and two-component co-SD DPIs for targeted pulmonary

nanomedicine are reported for the first time in this comprehensive and systematic study. The novel aspects of this study include organic solution advanced spray-drying in closed mode, the rational design and formulation of lung surfactant-mimic DPPC together with dipalmitoylphosphatidylethanolamine (DPPE)-PEG of varying PEG chain lengths as respirable dry powder particles, optimization for targeted pulmonary nanomedicine delivery as inhalable microparticles and nanoparticles in the solid state, and systematic comprehensive analyses. The rational design and optimization of these advanced dry powder inhalation aerosol nanomedicine formulations as aerosolized lung surfactant-mimic and lipopolymers as DPIs is important to allow for better understanding of the physicochemical properties and interactions of these particles formulated by advanced organic spray-drying and co-spray-drying processes in closed mode. To the authors' knowledge, this is the first report on a comprehensive and systematic study on the advanced formulation and characteristics of various combinations of DPPC and PEGylated phospholipids comprised of various PEG lengths for targeted pulmonary nanomedicine as inhaled dry powder aerosols.

Materials and methods

Materials

Synthetic DPPC (molecular weight 734.039 g/mol, >99% purity) and DPPE-PEG (molecular weights: 2749.391 g/mol, 3716.304 g/mol, and 5741.510 g/mol, which correspond to 2000, 3000, and 5000 molecular weight PEG lengths per compound; >99% purity) were obtained from Avanti Polar Lipids (Alabaster, AL). Their corresponding chemical structures are shown in Figure 1 (ChemSketch 12.01; Advanced Chemistry Development, Toronto, Canada). Methanol (high-performance liquid chromatography [HPLC] grade, American Chemical Society [ACS]-certified and chloroform [HPLC grade, ACS certified]) was obtained from Fisher Scientific (Pittsburgh, PA). Hydranal-Coulomat AD was from Sigma-Aldrich (St Louis, MO). Ultrahigh-purity (UHP) dry nitrogen gas was from Scott-Gross (Lexington, KY). All materials were used as stored in the freezer at –23°C and used as received.

Organic solution advanced spray-drying and co-spray-drying in closed mode from dilute solution

Advanced spray-drying of single-component DPPC and PEGylated phospholipids and co-spray drying of DPPC:PEGylated two-component systems from dilute organic solution was performed with a B-290 Büchi Mini Spray Dryer coupled with a B-295 Inert Loop and high-performance cyclone (all from Büchi Labortechnik, Flawil, Switzerland) in closed mode using UHP dry nitrogen gas as the atomizing gas. The feed solutions were prepared by dissolving various amounts of DPPC and/or DPPE-PEG in methanol to form dilute organic solutions of 0.1% w/v. Based on our previous organic solution advanced spray-drying work,[42] the following spray-drying conditions were used: atomization gas flow rate of 600 L/hour, aspiration rate of 35 m^3/hour, inlet temperature of 150°C (maintained in the first spray-drying process), and three different pump rates, designated as "low P," "med P," and "high P" pump rates, which corresponded to 3 mL/minute (10%), 15 mL/minute (50%), and 30 mL/minute (100%), respectively. Table 1 shows the various formulated particle systems and their corresponding DPPC and DPPE-PEG amounts and types, pump rates, and outlet temperatures (which represent the secondary drying

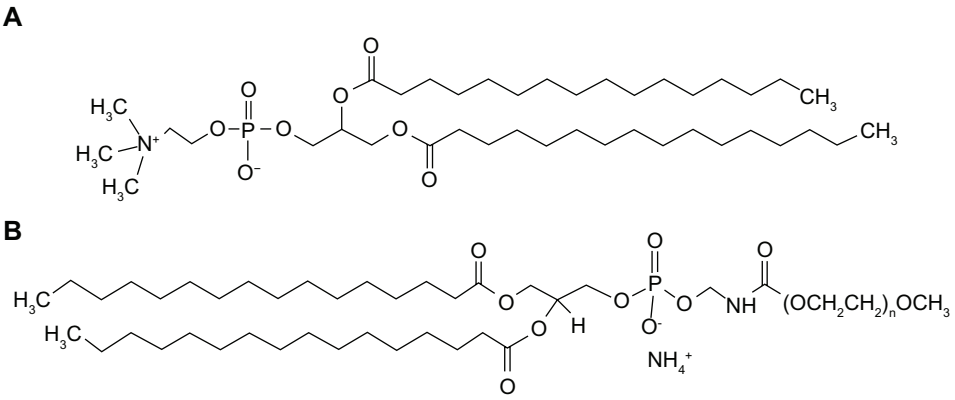

Figure 1 Chemical structures of (**A**) dipalmitoylphosphatidylcholine and (**B**) dipalmitoylphosphatidylethanolamine methoxy-poly(ethylene glycol).
Notes: n = 45, 67, and 113 for 2000, 3000, and 5000 MW poly(ethylene glycol), respectively, where n denotes the number of ethylene glycol oligomers present.

Table 1 Formulated spray-dried and co-spray-dried particle systems, their corresponding DPPC and/or DPPE-PEG amounts, and spray-drying conditions where low P, medium P, and high P correspond to 10%, 50%, and 100% pump rates, respectively

System	DPPC (mol%)	DPPE-PEG (mol% and PEG MW)	Pump rate (mL/minute) (%)	Outlet T (°C)
100 DPPC (low P)	100	0	3 (10%)	85
100 DPPC (medium P)	100	0	15 (50%)	70
100 DPPC (high P)	100	0	30 (100%)	49
95 DPPC:5 DPPE-PEG2k (low P)	95	5 (2k)	3 (10%)	71
95 DPPC:5 DPPE-PEG2k (medium P)	95	5 (2k)	15 (50%)	73
95 DPPC:5 DPPE-PEG2k (high P)	95	5 (2k)	30 (100%)	40
95 DPPC:5 DPPE-PEG3k (low P)	95	5 (3k)	3 (10%)	73
95 DPPC:5 DPPE-PEG3k (medium P)	95	5 (3k)	15 (50%)	79
95 DPPC:5 DPPE-PEG3k (high P)	95	5 (3k)	30 (100%)	43
95 DPPC:5 DPPE-PEG5k (low P)	95	5 (5k)	3 (10%)	69
95 DPPC:5 DPPE-PEG5k (medium P)	95	5 (5k)	15 (50%)	64
95 DPPC:5 DPPE-PEG5k (high P)	95	5 (5k)	30 (100%)	37

Abbreviations: DPPC, dipalmitoylphosphatidylcholine; DPPE, dipalmitoylphosphatidylethanolamine; PEG, poly(ethylene glycol).

process temperatures). The nozzle diameter (composed of stainless steel) was 0.7 mm, and the spray-dried particles were separated from the drying gas (UHP nitrogen) in the high-performance cyclone and collected in a sample collector. All SD and co-SD powders were stored in glass vials sealed with parafilm in glass desiccators over Drierite (Xenia, OH) desiccant in the freezer at −23°C under ambient pressure.

Scanning electron microscopy for morphology and shape analysis

The shape and surface morphology of particles was evaluated by scanning electron microscopy (SEM), using a Hitachi S-4300 microscope (Tokyo, Japan). Samples were placed on double-sided adhesive carbon tabs and were adhered to aluminum stubs (TedPella, Redding, CA) which were coated with a gold/palladium alloy thin film using an Emscope SC400 sputter coating system at 20 µA for 1 minute under argon gas. The electron beam with an accelerating voltage of 5–10 kV was used at a working distance of 13.3–15.3 mm. Images were captured at several magnifications.

Particle sizing and size distribution using SEM

The mean size, standard deviation, and size range of the particles were determined digitally using SigmaScan® 5.0 software (Systat, San Jose, CA). Representative micrographs for each particle sample at 5000× magnification were analyzed by measuring the diameter of at least 100 particles per image with the SigmaScan software.

Powder X-ray diffraction

Using similar conditions previously reported by the authors,[42] powder X-ray diffraction (PXRD) patterns of powder samples were measured by a Rigaku Multiflex X-ray diffractometer (The Woodlands, TX) with a slit-detector Cu Kα radiation source (40 kV, 44 mA, and $\lambda = 1.5406$ Å). The scan range was 5.0–50.0 2θ (°) with a scan rate of 2.0°/minute at ambient temperature. The sample was placed on a horizontal quartz glass sample holder plate.

Differential scanning calorimetry

Thermal analysis and phase-transition measurements were carried out using a TA Q200 differential scanning calorimetry (DSC) system (TA Instruments, New Castle, DE) equipped with T-Zero® technology and an automated computer-controlled RSC-90 cooling accessory. Using similar conditions previously reported by the authors,[42] 1–3 mg of powder was weighed into hermetic anodized aluminum T-Zero® DSC pans and were hermetically sealed with the T-Zero® hermetic sealer. UHP dry nitrogen gas was used as the purging gas at 50 mL/minute. The heating range was 0°C–250°C at a heating scan rate of 5.00°C/minute.

Karl Fischer coulometric titration

The water content of all powders was chemically quantified by Karl Fisher (KF) coulometric titration, using similar conditions previously reported by the authors.[42] The measurements were performed with a 737 KF Coulometer coupled with 703 Ti Stand (Metrohm, Antwerp, Belgium). Approximately 5 mg of powder was dissolved in a known volume of chloroform. The sample solution was injected into the reaction cell that

contained Hydranal KF reagent and the water content was then calculated from the resulting reading.

Attenuated total-reflectance fourier-transform infrared spectroscopy

Attenuated total-reflectance Fourier-transform infrared spectroscopy (ATR-FTIR) was performed using a Varian 7000e step-scan spectrometer (Agilent Technologies, Santa Clara, CA). The powder was placed on the diamond ATR crystal, covered with a glass coverslip, and held in place with a specialized clamp. ATR crystal and IR spectra were obtained at an 8 cm^{-1} spectral resolution between 700 and 4000 cm^{-1}. The data were collected and analyzed using Varian Resolutions software.

Hot-stage microscopy under cross-polarizers

Using similar conditions previously reported by the authors,[42] hot-stage microscopy (HSM) studies were completed using a BX51 polarized microscope (Olympus, Tokyo, Japan) equipped with an Instec STC200 heating unit and S302 hot stage (Boulder, CO). The polarized light was filtered by a γ 530 nm U-TP530 filter lens. Powder samples were mounted on a cover glass and heated from 25°C to 250°C at a heating scan rate of 5°C/minute. The heating program was controlled by WinTemp software, and images were digitally captured via a SPOT Insight digital camera (Diagnostic Instruments, Sterling Heights, MI).

Confocal Raman microscopy and spectroscopy

Confocal Raman microspectroscopy (CRM) was performed using an Aramis confocal dispersive Raman spectrometer and fluorescence microscope system (Horiba Jobin Yvon, Edison, NJ), using similar conditions previously reported by the authors.[43] The system is equipped with an Olympus BX41 confocal optical microscope and an Olympus U-LH 100 W Hg lamp and U-RFL-T power source used for fluorescence excitation and bright-field illumination. All optical images and Raman spectra were obtained using a 50× objective. Raman spectra and spectral maps were acquired using a 633 nm HeNe laser. Spectral maps were obtained with the stage moved in increments of 2 μm. Each map point was acquired using 2 seconds of detector exposure time, with 32 accumulations acquired per point using a grating of 600 grooves/mm and a center wavenumber of 1200 cm^{-1} (for spectra in the fingerprint region) and two accumulations acquired per point, with a grating of 950 grooves/mm and a center wavenumber of 2900 cm^{-1} (for the C–H stretching region). A confocal hole of 500 μm and a slit width of 100 μm were used. Spectra covering the range of 200–4000 cm^{-1} were obtained in automatic scanning mode using the 950 groove/mm grating. Spectra were subjected to baseline correction and smoothing prior to further analysis.

Aerosol dispersion performance analysis by Next Generation Impactor™ (NGI™)

In accordance with the *United States Pharmacopeia* chapter 601 specifications on aerosols,[44] the aerosol-dispersion properties of the dry powder particles as DPIs were determined using the Next Generation Impactor™ (NGI™) with a stainless steel induction port (ie, United States Pharmacopeia throat) attachment (model 170; MSP, Shoreview, MN), equipped with specialized stainless steel NGI™ gravimetric insert cups (MSP). The NGI™ was coupled with a Copley TPK 2000 critical flow controller (Copley Scientific, Nottingham, UK), which was connected to an HCP5 vacuum pump (Copley Scientific). The airflow rate, Q, was measured and adjusted prior to each experiment using a DFM 2000 flow meter (Copley Scientific).

The aerosolization studies were experimentally designed by Design Expert® 8.0.7.1 software (Stat-Ease, Minneapolis, MN). Glass-fiber filters (55 mm, type A/E; Pall Life Sciences, Exton, PA) were placed in the stainless steel NGI™ gravimetric insert cups for NGI™ stages 1–7 to minimize bounce or reentrapment.[45] Three hydroxypropyl methylcellulose hard capsules (size 3, Quali-V®; Qualicaps, Whitsett, NC) were each loaded with 10 mg of powder and were then loaded into a high-resistance (ie, high sheer stress) human DPI device, the HandiHaler® (Boehringer Ingelheim, Ridgefield, CT), and tightly inserted into the induction port. The NGI™ was run at a controlled flow rate at Q = 60 L/minute with a delay time of 10 seconds (NGI™ Flow controller) prior to the capsules being needle-pierced open by the HandiHaler® mechanism, where the particles were then drawn into the inertial impactor for 10 seconds. This was done with a total of three capsules per sample for a total of 30 mg total per run. For each 30 mg run, the amount of particles deposited onto each stage was determined gravimetrically by measuring the difference in mass of the glass filters after particle deposition. For the NGI™ Q = 60 L/minute, the effective cutoff diameters for each impaction stage were calibrated by the manufacturer and stated as: Stage 1 (8.06 μm); Stage 2 (4.46 μm); Stage 3 (2.82 μm); Stage 4 (1.66 μm); Stage 5 (0.94 μm); Stage 6

(0.55 μm); and Stage 7 (0.34 μm). The fine particle dose (FPD), fine particle fraction (FPF), respirable fraction (RF), and emitted dose (ED) were calculated as follows:

$$\text{FPD} = \text{mass of particles} < 4.4\ \mu\text{m (stages 2–7)}$$

$$\text{FPF} = \frac{\text{Fine particle dose}}{\text{Initial particle mass loaded into capsules}} \times 100\%$$

$$\text{RF} = \frac{\text{Mass of particles} < 4.4\ \mu\text{m (stages 2 through 7)}}{\text{Total particle mass on all stages}} \times 100\%$$

$$\text{ED} = [(\text{initial mass in capsules} - \text{final mass remaining in capsules}) / \text{initial mass in capsules}] \times 100\%$$

The mass mean aerodynamic diameter (MMAD) and geometric standard deviation (GSD) were determined using a mathematical program written by Dr Warren Finlay. All experiments were triplicated (n = 3).

Results

SEM, particle sizing, and size distribution

Formulated particle and surface morphologies were visualized and analyzed via SEM. Figures 2–5 include SEM micrographs of the particles at 10,000× and corresponding raw DPPC or DPPE-PEG at 1000×. Their corresponding size (diameter), standard deviation, and range are exhibited in Table 2, as determined using SigmaScan® software. 100 DPPC (pure one-component DPPC)-formulated particles are smooth and spherical, and their diameter increased with increasing pump rate (diameters of 0.642 ± 0.188, 0.790 ± 0.292, and 0.960 ± 0.499 μm for low P, medium P, and high P, respectively). Formulated 95 DPPC:5 DPPE-PEG2k particle size also increased with increasing pump rate; however, only the high P formulation exhibited spherical morphology and a diameter of 1.166 ± 0.676 μm. Low P and high P particle systems were rough and agglomerated, and their diameter could not be determined. Similarly, 95 DPPC:5 DPPE-PEG3k and 95 DPPC:5 DPPE-PEG5k formulated particle sizes increased with increasing pump rate, and the high P formulations were spherical with diameters of 1.200 ± 0.931 μm and 1.161 ± 0.595 μm, respectively. The low P and medium P formulations for both systems were agglomerated and rough, and their diameters were not determined. Also, the surface roughness of the high P particle formulations seemed to be rough. This was a result of charging of the particles during SEM, as their initial morphology

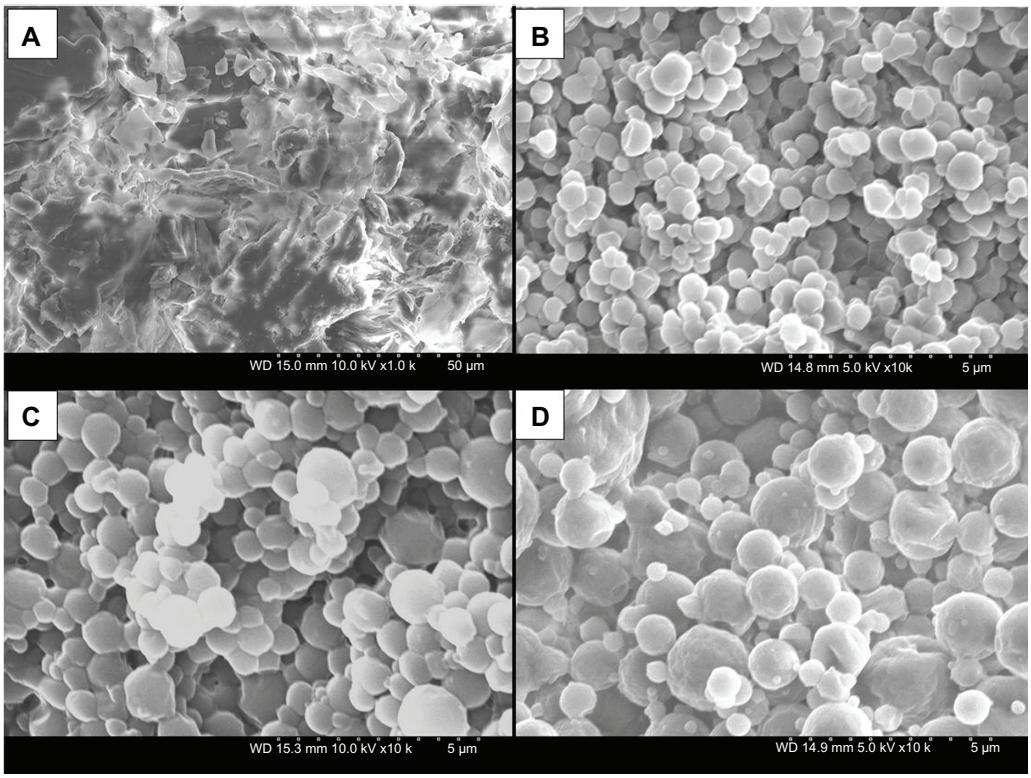

Figure 2 (**A**–**D**) Scanning electron micrographs of raw dipalmitoylphosphatidylcholine (DPPC) and spray-dried 100 DPPC particles at three pump rates. (**A**) Raw DPPC, magnification 1000×; (**B**) DPPC particles at 10% (low P) pump rate, magnification 10,000×; (**C**) DPPC particles at 50% (medium P) pump rate, magnification 10,000×; (**D**) DPPC particles at 100% (high P) pump rate, magnification 10,000×.

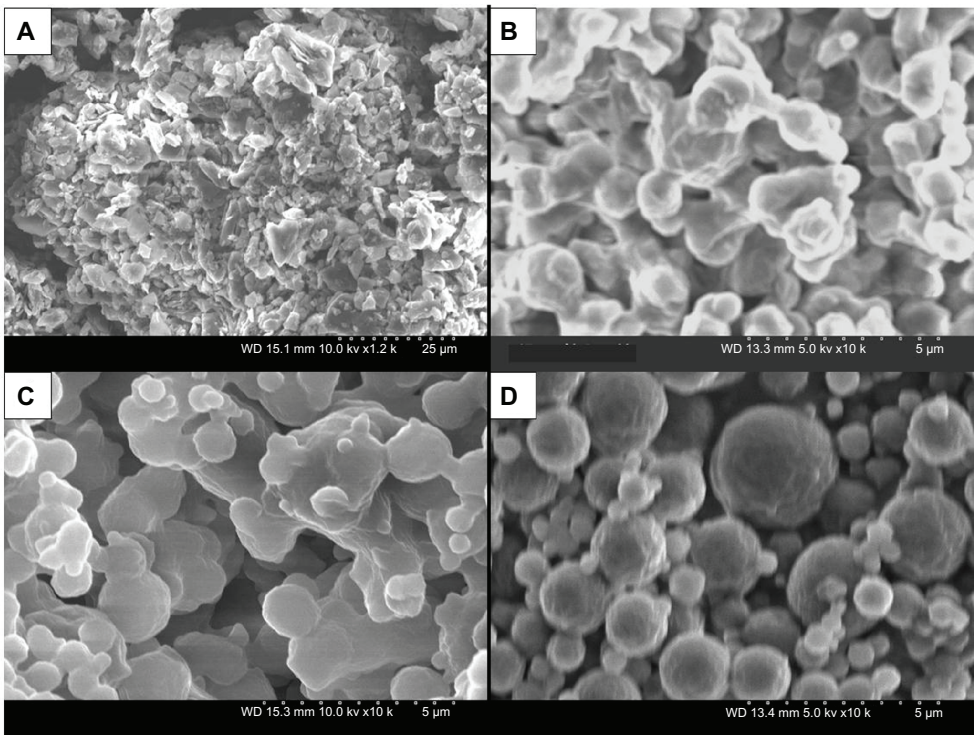

Figure 3 (**A**–**D**) Scanning electron micrographs of raw dipalmitoylphosphatidylethanolamine poly(ethylene glycol)-2k 95 DPPC:5 DPPE-PEG2k and co-spray-dried 95 dipalmitoylphosphatidylcholine (DPPC):5 DPPE-PEG 2k particles at three pump rates. (**A**) Raw DPPE-PEG2k, magnification 1000×; (**B**) 95 DPPC:5 DPPE-PEG2k particles at 10% (low P) pump rate, magnification 10,000×; (**C**) 95 DPPC:5 DPPE-PEG2k particles at 50% (medium P) pump rate, magnification 10,000×; (**D**) 95 DPPC:5 DPPE-PEG2k particles at 100% (high P) pump rate, magnification 10,000×.

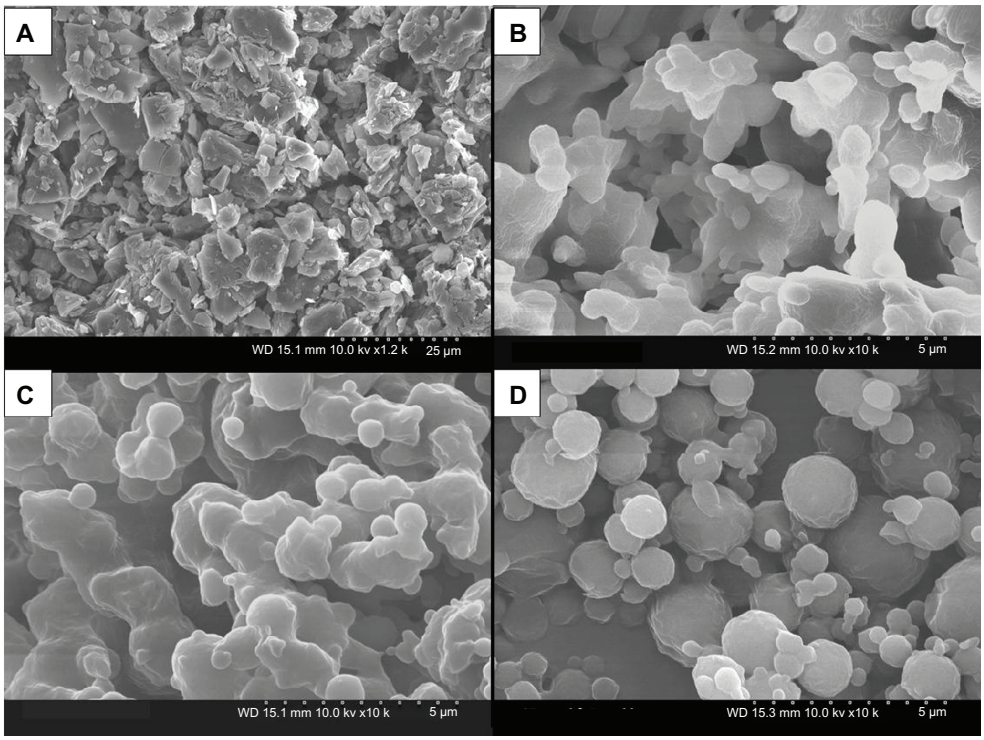

Figure 4 (**A**–**D**) Scanning electron micrographs of raw dipalmitoylphosphatidylethanolamine poly(ethylene glycol)-3k (DPPE-PEG3k) and co-spray-dried 95 dipalmitoylphosphatidylcholine (DPPC):5 DPPE-PEG3k particles at three pump rates. (**A**) Raw DPPE-PEG3k, magnification 1000×; (**B**) 95 DPPC:5 DPPE-PEG3k particles at 10% (low P) pump rate, magnification 10,000×; (**C**) 95 DPPC:5 DPPE-PEG3k particles at 50% (medium P) pump rate, magnification 10,000×; (**D**) 95 DPPC:5 DPPE-PEG3k particles at 100% (high P) pump rate, magnification 10,000×.

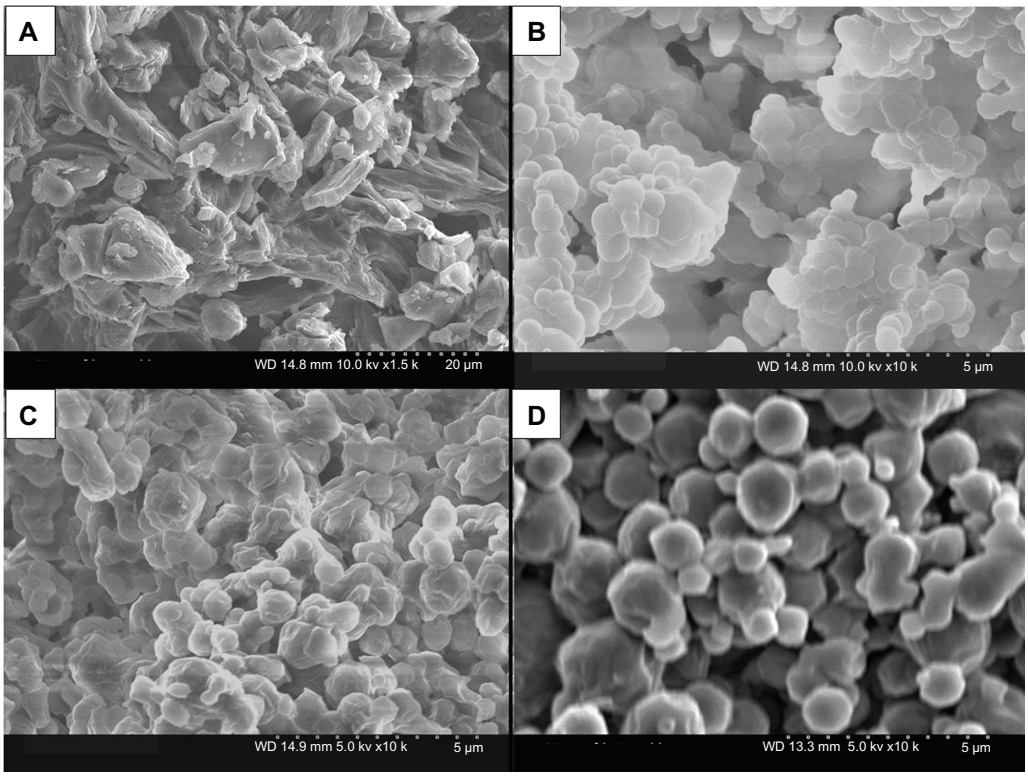

Figure 5 (**A**–**D**) Scanning electron micrographs of raw dipalmitoylphosphatidylethanolamine poly(ethylene glycol)-5k (DPPE-PEG5k) and co-spray-dried 95 dipalmitoylphosphatidylcholine (DPPC):5 DPPE-PEG 5k particles at three pump rates. (**A**) Raw DPPE-PEG5k, magnification 1000×; (**B**) 95 DPPC:5 DPPE-PEG 5k particles at 10% (low P) pump rate, magnification 10,000×; (**C**) 95 DPPC:5 DPPE-PEG 5k particles at 50% (medium P) pump rate, magnification 10,000×; (**D**) 95 DPPC:5 DPPE-PEG 5k particles at 100% (high P) pump rate, magnification 10,000×.

prior to image capture was smooth and spherical. Overall, the particle sizes exhibited by all formulated microparticulate/nanoparticulate powders were in the respirable size range.

Powder X-ray diffraction

Powder X-ray diffractograms (Figure 6) showed the presence of a strong peak at 21° 2Θ for both raw DPPC and all formulated 100 DPPC particles, which corresponds to the presence of the lipid bilayer.[37] Raw DPPE-PEG showed the presence of strong peaks at 19° and 23° 2Θ, a small peak at 21° 2Θ, and smaller broad peaks above 25° 2Θ. The peaks at 19°, 23°, and above 25° 2Θ are similar to previous results for PEG powder,[46] whereas the peak at 21° 2Θ corresponds to the presence of a phospholipid bilayer. Upon spray-drying, the peaks above 25° 2Θ disappeared, whereas the peaks at 19° and 23° 2Θ remained for all formulated particle systems. Furthermore, the peak present at 21° 2Θ increased due to the influence of DPPC in the particle formulation. Although there was no correlation in peak intensity with spray-drying pump rates, the intensity of the peaks corresponding to PEG increased with increasing PEG chain length for the raw DPPE-PEG compounds.

Table 2 Particle-size parameters of spray-dried DPPC and co-spray-dried DPPC:DPPE-PEG particles (mean ± standard deviation)

System	Diameter (µm)	Range (µm)
100 DPPC (low P)	0.642 ± 0.188	0.274–1.157
100 DPPC (medium P)	0.790 ± 0.292	0.228–1.755
100 DPPC (high P)	0.960 ± 0.499	0.220–2.000
95 DPPC:5 DPPE-PEG2k (high P)	1.166 ± 0.676	0.360–4.068
95 DPPC:5 DPPE-PEG3k (medium P)	1.049 ± 0.529	0.303–3.775
95 DPPC:5 DPPE-PEG3k (high P)	1.200 ± 0.931	0.034–5.298
95 DPPC:5 DPPE-PEG5k (medium P)	0.837 ± 0.299	0.316–1.759
95 DPPC:5 DPPE-PEG5k (high P)	1.161 ± 0.595	0.326–2.966

Abbreviations: DPPC, dipalmitoylphosphatidylcholine; DPPE, dipalmitoylphosphatidylethanolamine; PEG, poly(ethylene glycol).

Differential scanning calorimetry

DSC thermograms for formulated particles and their corresponding raw counterparts can be seen in Figure 7. Raw DPPC exhibited three endothermic peaks, including a crystal-to-gel (T_c) bilayer phase transition at ~47.1°C, pretransition peak corresponding to a gel-to-ripple (T_p) phase at ~67.0°C, and the bilayer main phase transition (T_m) to the liquid crystalline phase at ~72.0°C, where the hydrophobic acyl chain core

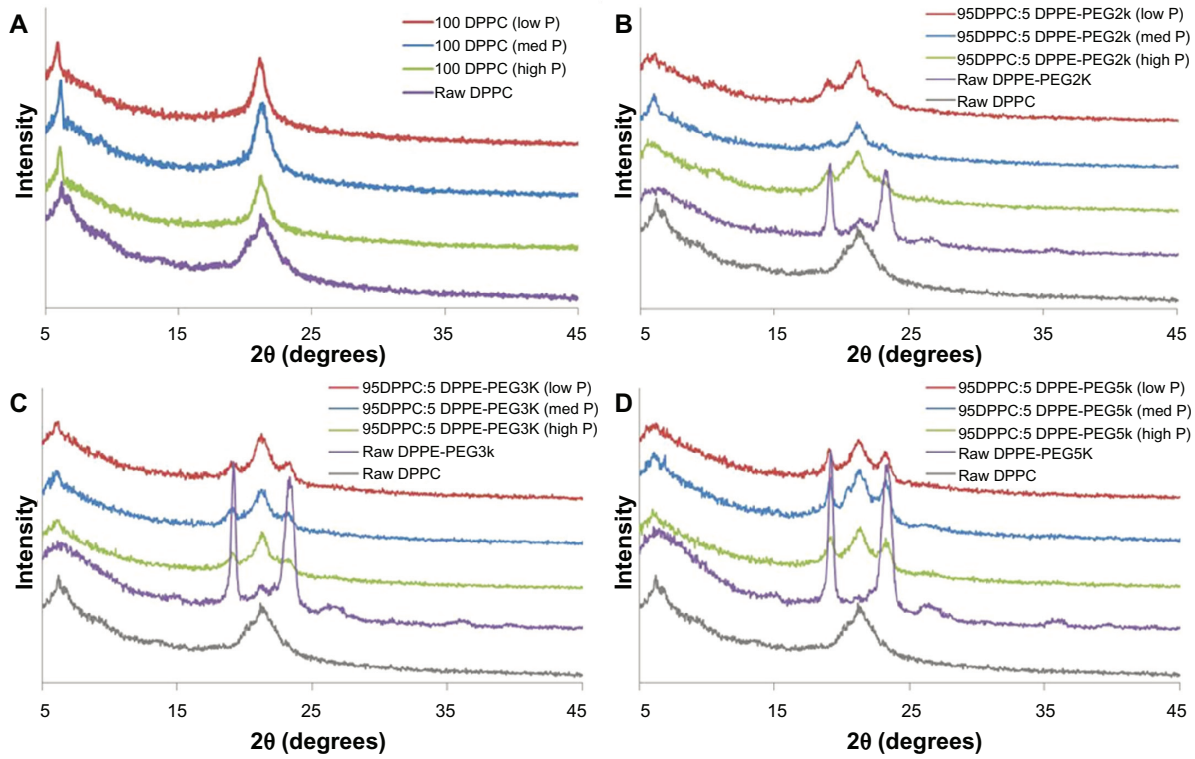

Figure 6 Powder X-ray diffractograms of: (**A**) formulated spray-dried (SD) dipalmitoylphosphatidylcholine (DPPC) particles at three pump rates versus raw DPPC; (**B**) formulated co-SD DPPC: dipalmitoylphosphatidylethanolamine poly(ethylene glycol)-2k (DPPE-PEG2k) particles at three pump rates versus raw DPPC and raw DPPE-PEG2k; (**C**) formulated co-SD DPPC:DPPE-PEG3k particles at three pump rates versus raw DPPC and raw DPPE-PEG3k; (**D**) formulated co-SD DPPC:DPPE-PEG5k particles at three pump rates versus raw DPPC and raw DPPE-PEG5k.
Note: Low P, med P, and high P correspond to 10%, 50%, and 100% pump rates, respectively.

melted. This is consistent with our earlier findings on raw DPPC powder.[24] The phase behavior of solid-state DPPC, fully hydrated DPPC, and at varying levels of water content in the solid state have been previously reported by the authors.[24–26] Formulated 100 DPPC particles exhibited the characteristic bilayer main transition phase (T_m) at ~68°C, which corresponds to the bilayer main transition phase of raw DPPC confirming the presence of the phospholipid bilayer. The bilayer phase temperatures for SD DPPC were slightly lower than that of the raw DPPC, and it was determined that the heat of fusion of the formulated particles increased with increasing pump rate (24.8, 29.2, and 36.1 J/g for low P, medium P, and high P, respectively). Neither T_c nor T_p were observed in the thermograms for the SD DPPC particles, indicating that spray-drying rendered the bilayers in the gel state (not the crystalline state, as was observed with raw DPPC). All DPPC systems underwent decomposition around 160°C.

Raw DPPE-PEG2k exhibited two endothermic peaks, including a pretransition peak at 43.5°C and main phase transition at ~52.1°C. The co-SD 95 DPPC:5 DPPE-PEG2k particle systems exhibited two endothermic peaks: the first around 47°C, which corresponds to the DPPE-PEG main phase transition (T_c), and the second in the range of 70°C–75°C, which corresponds to the DPPC bilayer main phase transition – T_m. Furthermore, the low P sample exhibited a third endotherm near 90°C. Raw DPPE-PEG3k exhibited a single endothermic peak at 52.0°C, corresponding to the main phase transition. The 95 DPPC:5 DPPE-PEG3k particles exhibited two endothermic peaks near 49.5°C (corresponding to the DPPE-PEG3k transition phase) and 74°C (corresponding to the DPPC bilayer phase transition). For the DPPC bilayer phase transition peaks, the heat of fusion increased with increasing pump rate at 2.0, 10.7, and 17.0 J/g for low P, medium P, and high P, respectively. The low P particles had a third endotherm near 100°C. Similarly, raw DPPE-PEG5k exhibited a pretransition peak at 48.3°C and main phase transition at 57.9°C. The 95 DPPC:5 DPPE-PEG5k particles showed two endothermic peaks at 55.3°C and 73°C, which corresponded to the main phase transition of DPPE-PEG5k and DPPC, respectively. For the DPPC bilayer phase transition peaks, the heat of fusion increased with increasing pump rate at 2.6, 11.0, and 14.7 J/g for low P, medium P, and high P, respectively. The low P particles had a third endotherm near 100°C.

For the main phase transition temperatures corresponding to the DPPE-PEG peaks (first endotherms for formulated

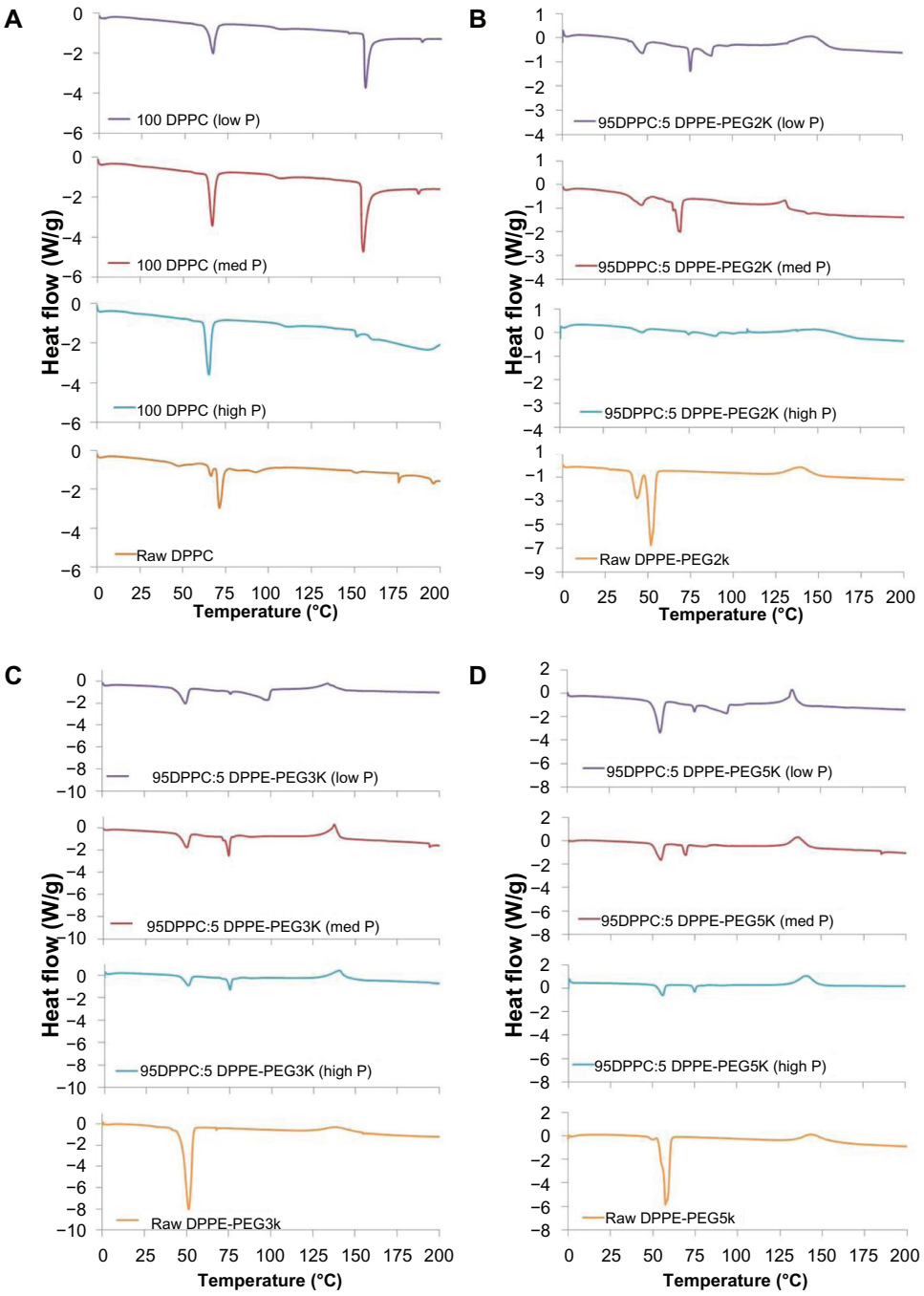

Figure 7 Differential scanning calorimetry thermograms of: (**A**) formulated spray-dried (SD) dipalmitoylphosphatidylcholine (DPPC) particles at three pump rates versus raw DPPC; (**B**) formulated co-SD DPPC:dipalmitoylphosphatidylethanolamine poly(ethylene glycol)-2k (DPPE-PEG2k) particles at three pump rates versus raw DPPE-PEG2k; (**C**) formulated co-SD DPPC:DPPE-PEG3k particles at three pump rates versus raw DPPE-PEG3k; (**D**) formulated co-SD DPPC:DPPE-PEG5k particles at three pump rates versus raw DPPE-PEG5k.

Note: Low P, med P, and high P correspond to 10%, 50%, and 100% pump rates, respectively.

co-SD DPPC:DPPE-PEG particles), the temperature increased with increasing PEG molecular weight. Also, the peaks corresponding to DPPE-PEG in the formulated co-SD powders are broader and result in high heats of fusion in comparison to the DPPC-related peaks. Furthermore, all formulated co-SD 95 DPPC:5 DPPE-PEG and raw DPPE-PEG samples decomposed above 130°C.

Karl Fischer coulometric titration

The residual water content in the solid state of the formulated particles and their raw components are shown in Table 3. The water content of raw DPPC was 1.74% ± 0.15% (w/w) and ranged from 4.59% to 5.17% (w/w) for SD 100 DPPC particles. The water content for raw DPPE-PEG2k was 0.70% ± 0.21% (w/w) and ranged from 1.29% to 3.13%

Table 3 Water content of formulated spray-dried DPPC and co-spray-dried DPPC:DPPE-PEG particles and their raw counterparts analyzed via Karl Fischer coulometric titration (mean ± standard deviation, n = 3)

System	Water% (w/w)
100 DPPC (low P)	4.93 ± 1.29
100 DPPC (medium P)	4.59 ± 1.03
100 DPPC (high P)	5.17 ± 1.29
Raw DPPC	1.74 ± 0.15
95 DPPC:5 DPPE-PEG2k (low P)	1.29 ± 0.70
95 DPPC:5 DPPE-PEG2k (medium P)	3.13 ± 1.17
95 DPPC:5 DPPE-PEG2k (high P)	1.76 ± 0.83
Raw DPPE-PEG2k	0.70 ± 0.21
95 DPPC:5 DPPE-PEG3k (low P)	2.43 ± 0.60
95 DPPC:5 DPPE-PEG3k (medium P)	2.82 ± 0.89
95 DPPC:5 DPPE-PEG3k (high P)	4.34 ± 1.71
Raw DPPE-PEG3k	0.60 ± 0.12
95 DPPC:5 DPPE-PEG5k (low P)	1.46 ± 0.75
95 DPPC:5 DPPE-PEG5k (medium P)	1.65 ± 0.26
95 DPPC:5 DPPE-PEG5k (high P)	3.11 ± 1.11
Raw DPPE-PEG5k	1.04 ± 0.65

Note: Low P, medium P, and high P correspond to 10%, 50%, and 100% pump rates, respectively.
Abbreviations: DPPC, dipalmitoylphosphatidylcholine; DPPE, dipalmitoylphosphatidylethanolamine; PEG, poly(ethylene glycol).

(w/w) for formulated co-SD 95 DPPC:5 DPPE-PEG2k particles. For raw DPPE-PEG3k, the water content was 0.60% ± 0.12% (w/w) and for formulated co-SD 95 DPPC:5 DPPE-PEG3k, particles ranged from 2.82% to 4.34% (w/w). Finally, the water content for raw DPPE-PEG5k was 1.01% ± 0.65% (w/w), whereas it ranged from 1.46% to 3.11% (w/w) for the formulated co-SD 95 DPPC:5 DPPE-PEG5k particles. There was no trend in the water-content values for formulated systems based on the spray-drying pump rates or type of DPPE-PEG used. All water-content values were low and well within an acceptable range for inhalable dry powder formulations.

Cross-polarizing light hot-stage microscopy

Representative micrographs of raw DPPE-PEG3k and formulated co-SD 95 DPPC:5 DPPE-PEG3k (high P) particles are shown in Figures 8 and 9, respectively. Raw DPPE-PEG3k showed dark agglomerates lacking birefringency between 25°C and 55°C, which indicated a noncrystalline, amorphous material. A phase transition was visualized by HSM near 57°C to 58°C, which likely corresponded to the gel to liquid-crystal transition, as shown in the DSC thermogam at 52°C for raw DPPE-PEG3k in Figure 7C. Melting was visualized starting at 60°C by the formation of liquid droplets, with decomposition occuring above 150°C.

The micrographs for co-SD 95 DPPC:5 DPPE-PEG3k (high P) particles also showed dark agglomerates lacking birefringency between 25°C and 100°C, which indicated a noncrystalline, amorphous material. No visible phase transition was evident and melting started around 115°C, as shown by liquid droplet formation. Decomposition was evident above 185°C. This behavior corresponds closely to that observed for raw DPPC (data not shown), which is the primary component of these particles.

Attenuated total-reflectance fourier-transform infrared spectroscopy

Formulated particles and their raw counterparts underwent ATR-FTIR analysis to determine the functional groups present in the systems, as shown in Figure 10. For both the raw DPPC and SD 100 DPPC particles, the spectra indicated the same characteristic peaks for all systems and were the same as in previously reported literature.[47] The spectra for formulated co-SD 95 DPPC:5 DPPE-PEG particles, however, exhibited peaks corresponding to DPPC and/or DPPE-PEG. Interestingly, the characteristic peaks shown for raw DPPE-PEG were the same as previously shown for pure PEG,[48] showing the strong influence of the PEG presence in the analysis of these systems. Although there is the absence of a broad water peak (3200–3400 cm^{-1}) for the raw DPPE-PEGs, this peak was present in both the raw DPPC and SD 100 DPPC particles as well as the formulated co-SD 95 DPPC:5 DPPE-PEG particles. While certain peaks relating to characteristic functional groups relate to DPPC or DPPE-PEG only, some are shared by both and have an influence on the formulated co-SD DPPC:DPPE-PEG particles. For instance, peaks present in the formulated DPPC:DPPE-PEG particles that are due to the influence of DPPC include those at 2924 cm^{-1} ($–CH_2$ antisymmetrical stretching), 2852 cm^{-1} ($–CH_2$ symmetrical stretching), 1250–1350 cm^{-1} (P=O stretching), and 721 cm^{-1} ($–N^+[CH_3]_3$ symmetrical stretching). Peaks due to the influence of DPPE-PEG (PEG) include 2870 cm^{-1} ($–CH_3$ symmetrical stretching), 1342 cm^{-1} (alcohols), and 1276 cm^{-1} (ethers). Peaks in the formulated particles due to the influence of DPPC and/or DPPE-PEG (present in all three) include 1720–1735 cm^{-1} (C–O ester stretching), 1465 cm^{-1} ($–CH_2$ deformation, 1050–1150 cm^{-1} (–C–C–) and 960 cm^{-1} ($–N^+[CH_3]_3$) antisymmetrical stretching).

Confocal Raman microscopy and chemical imaging

Confocal Raman microscopy (CRM) and chemical imaging was performed first on raw DPPC for comparison with formulated SD DPPC particles. The results are shown in Figure 11. The full-range Raman spectra obtained via the microscope

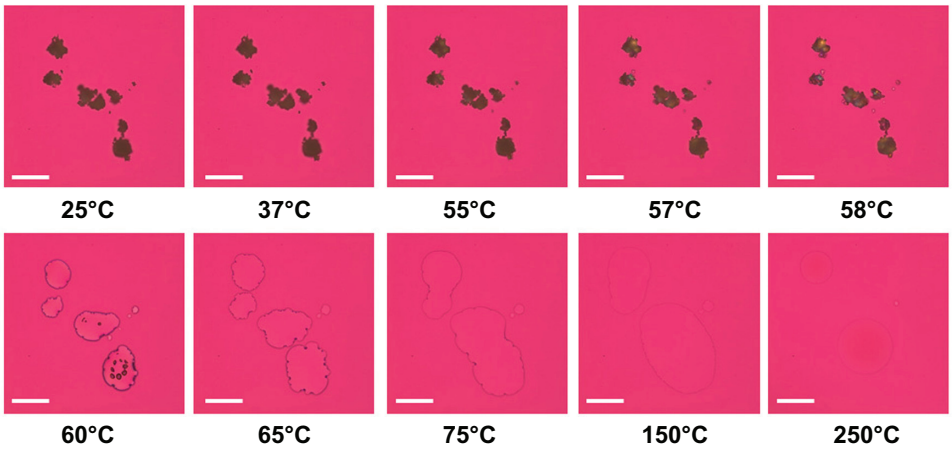

Figure 8 Representative hot-stage micrographs for raw dipalmitoylphosphatidylethanolamine poly(ethylene glycol)-3k.
Note: Scale bar = 3 mm.

at several different points showed no difference between the raw and SD DPPC, as seen in the selected spectra shown in Figure 11A. Two 32 × 32 maps were made at regions of the Raman spectrum centered at 2900 and 1200 cm^{-1}. A representative map of the region between 1400 and 1520 cm^{-1} is shown in Figure 11B and illustrates the observed results. The intensity variation observed in the red map was minor and showed no evidence of inhomogeneity within the particle. The variation is likely caused by sample height effects and minor density variations within the particle.

Raman microscopy and chemical imaging was also used to assess the homogeneity of formulated co-SD 95 DPPC:5 DPPE-PEG2k (high P) particles. Bands were identified that were specific for DPPC and DPPE-PEG2k, as shown in Figure 12A. Two regions were selected that were specific for DPPE-PEG2k, between 270 and 295 cm^{-1} and between 1225 and 1250 cm^{-1}. For DPPC, a band at 700 and 740 cm^{-1} was chosen. The areas of these bands were extracted from a 32 × 32 Raman spectral map, and are shown in Figure 12B–D. The blue, green, and red maps align with the bands denoted by colored arrowheads in Figure 12A. The map intensity observed for the selected bands, which are specific to the two chemical components of the particle, is seen to correlate between the three maps, indicating that DPPC and DPPE-PEG2k are similarly distributed in the particle at the resolution limit of Raman microscopy. Variations in the band area are caused by sample height effects and density variations within the mapped particle. Formulated co-SD 95 DPPC:5 DPPE-PEG3k (high P) particles were examined in a similar manner using the same set of Raman bands, leading to the results shown in Figure 13. Again, the colored maps correlate with each other and indicate that DPPC and DPPE-PEG3k are distributed similarly. Formulated 95 DPPC:5 DPPE-PEG5k (high P) particles were also examined using the

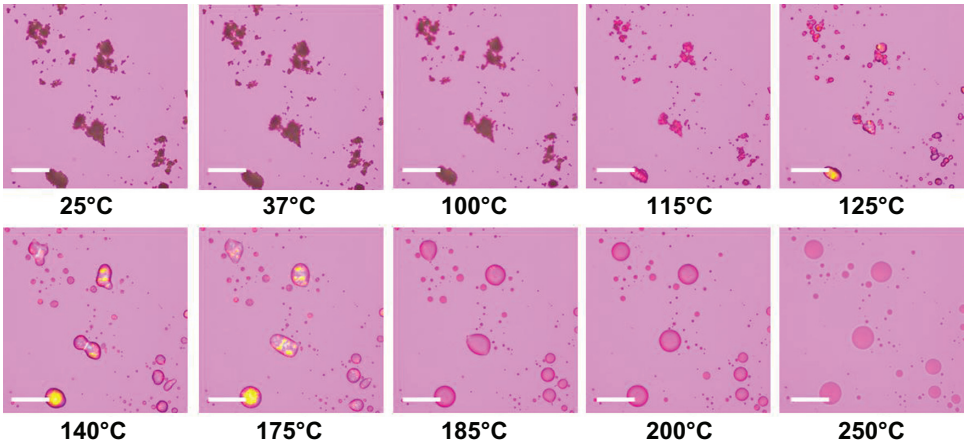

Figure 9 Representative hot-stage micrographs for co-spray-dried 95 dipalmitoylphosphatidylcholine:5 dipalmitoylphosphatidylethanolamine poly(ethylene glycol)-3k (high P) particles.
Note: Scale bar = 3 mm.

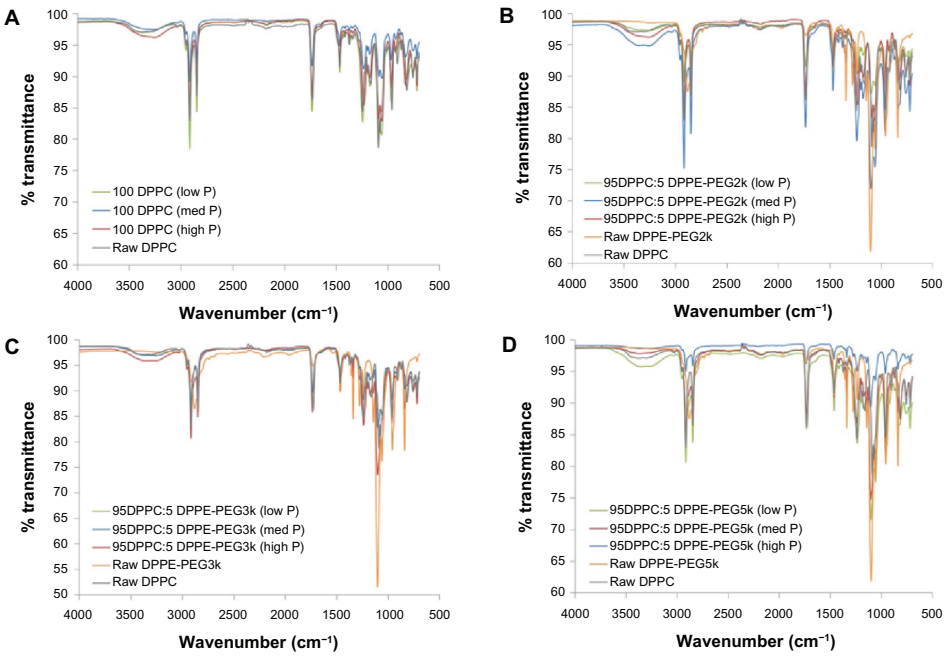

Figure 10 Attenuated total-reflectance Fourier-transform infrared spectra of: (**A**) formulated spray-dried (SD) dipalmitoylphosphatidylcholine (DPPC) particles at three pump rates versus raw DPPC; (**B**) formulated co-SD DPPC:dipalmitoylphosphatidylethanolamine poly(ethylene glycol)-2k (DPPE-PEG2k) particles at three pump rates versus raw DPPC and raw DPPE-PEG2k; (**C**) formulated co-SD DPPC:DPPE-PEG3k particles at three pump rates versus raw DPPC and raw DPPE-PEG3k; (**D**) formulated co-SD DPPC:DPPE-PEG5k particles at three pump rates versus raw DPPC and raw DPPE-PEG5k.
Note: Low P, med P, and high P correspond to 10%, 50%, and 100% pump rates, respectively.

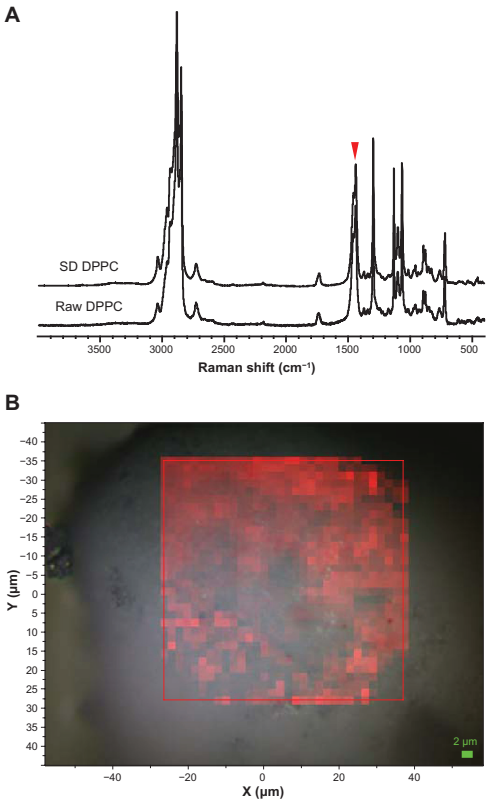

Figure 11 (**A**) Raman spectra obtained via confocal microscopy of raw dipalmitoylphosphatidylcholine (DPPC) and formulated spray-dried (SD) DPPC at 100% pump rate. The colored arrowhead shows the mapped bands. (**B**) Raman spectroscopic mapping showing the area of the Raman bands between 1400 and 1520 cm^{-1} (brighter-red colors indicate greater area) superimposed on a bright-field optical image of the surface of a particle of formulated SD DPPC (100% pump rate).

same approach, as shown in Figure 14, and also indicated a homogenous distribution of DPPC and DPPE-PEG5k.

Aerosol dispersion performance analysis using the Next Generation Impactor™ (NGI™)

The aerosol properties of the formulated particles produced at the highest pump rate (high P) were evaluated using an NGI coupled with the HandiHaler® DPI device (FDA-approved). The MMAD and geometric standard deviation values were similar for all four systems that were analyzed, ranging between 4.0 and 4.5 μm and 2.1 and 2.7 μm, respectively. The fine-particle dose increased upon using PEGylated phospholipids where SD 100 DPPC was 23.8% and co-SD 95 DPPC:5 DPPE-PEG2k, 3k, and 5k were 29.4%, 30.2%, and 29.5%, respectively. The ED was similar for all four systems, ranging from 91.2% to 94.2%, whereas the RF% increased with increasing PEGylation of the particles. These RF% values were 60.3% for SD 100 DPPC and co-SD 95 DPPC:5 DPPE-PEG2k, 3k, and 5k were at 68.7%, 71.7% and 75.5%, respectively. Figure 15 demonstrates the actual aerosol dispersion performance of the engineered dry powder microparticulate/nanoparticulate aerosols showing the % deposition on each NGI™ stage. Aerosol deposition on each NGI™ stage is measured, and in particular deposition on the lower stages of stage 2 all the way to stage 7 (lowest stage) is observed.

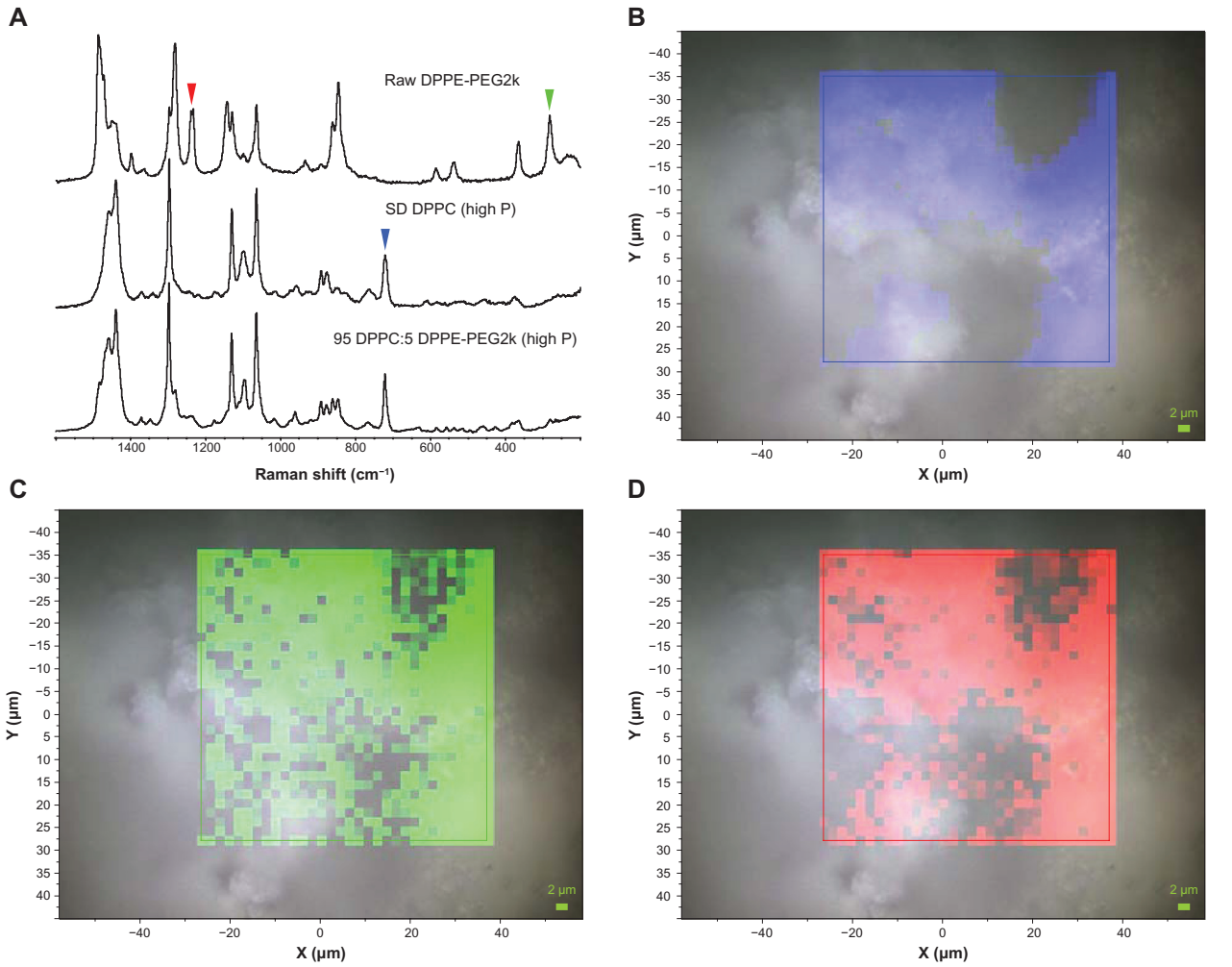

Figure 12 (**A**) Raman spectra obtained via confocal microscopy of raw dipalmitoylphosphatidylethanolamine poly(ethylene glycol)-2k (DPPE-PEG2k), formulated spray-dried (SD) dipalmitoylphosphatidylcholine (DPPC), and formulated co-SD 95 DPPC:5 DPPE-PEG2k (high P). Colored arrowheads show mapped bands. (**B**) Raman spectroscopic mapping showing the area of the Raman bands between 700 and 740 cm^{-1} (brighter colors indicate greater area) superimposed on a bright-field optical image of the surface of a particle of formulated SD DPPC (100% pump rate). (**C**) Map showing the area of the Raman bands between 270 and 295 cm^{-1}. (**D**) Map showing the area of the Raman bands between 1225 and 1250 cm^{-1}.

Discussion

This comprehensive and systematic study illustrates the physicochemical properties of DPPC and DPPC:DPPE-PEG microparticles and nanoparticles rationally designed for the first time by an organic solution closed-mode advanced spray-drying. Furthermore, this study also demonstrates for the first time their aerosol dispersion performance as DPIs for targeted pulmonary nanomedicine delivery, with excellent properties for high aerosol dispersion performance as dry powder inhalation aerosols. A systematic experimental design resulted in the successful design, development, and optimization of twelve particle systems, which included pure one-component SD DPPC particles and two-component co-SD 95 mole% DPPC:5 mole% DPPE-PEG DPI particles (using three different PEG chain lengths) at three different pump rates. This study strived to elucidate the effects of the presence of DPPE-PEG, PEG chain length, and the effects of the pump rate.

Overall, the use of dilute organic solution (such as alcohols, which are considered "green" chemicals) imparts a smaller primary droplet size by virtue of lower surface tension in the range of 20–25 mN/m (in contrast to water, which has a high surface tension of 72 mN/m and hence produces larger primary droplets) with rationally designed advanced spray-drying conditions resulted in the optimization of particle characteristics necessary for effective dry powder delivery. In addition, organic solution advanced spray-drying in closed mode eliminates the need for water and minimizes the residual water content in the final powder. This is an important and novel aspect reported here, as minimizing the residual water content in the solid state improves aerosol dispersion performance and promotes solid-state stability.

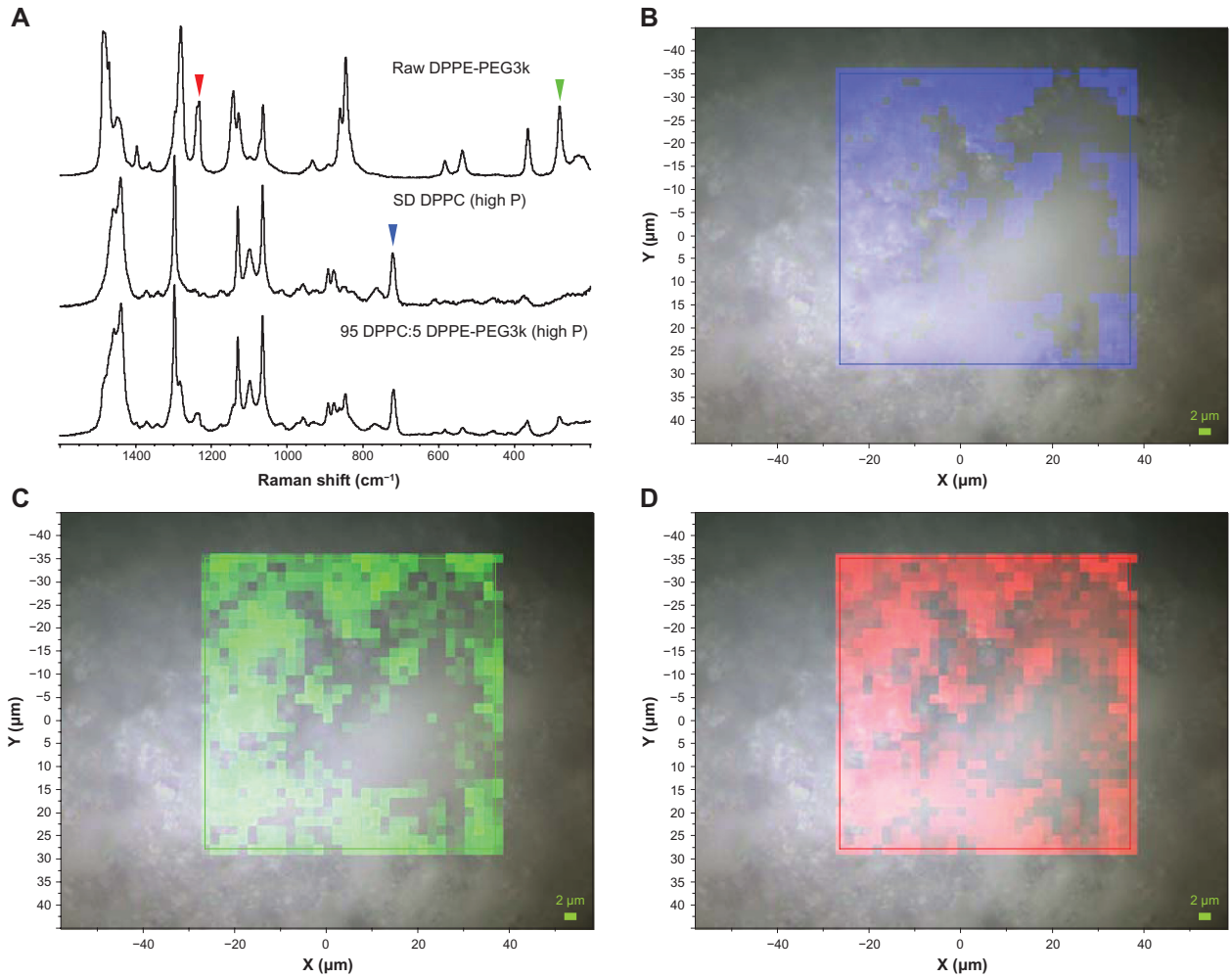

Figure 13 (**A**) Raman spectra obtained via confocal microscopy of raw dipalmitoylphosphatidylethanolamine poly(ethylene glycol)-3k (DPPE-PEG3k), formulated spray-dried (SD) dipalmitoylphosphatidylcholine (DPPC), and formulated co-SD 95 DPPC:5 DPPE-PEG3k (high P). Colored arrowheads show mapped bands. (**B**) Raman spectroscopic mapping showing the area of the Raman bands between 700 and 740 cm^{-1} (brighter colors indicate greater area) superimposed on a bright-field optical image of the surface of a particle of formulated SD DPPC (100% pump rate). (**C**) Map showing the area of the Raman bands between 270 and 295 cm^{-1}. (**D**) Map showing the area of the Raman bands between 1225 and 1250 cm^{-1}.

SEM analysis showed that the particles exhibited an ideal size range (0.5–1.5 µm), which is comparable to respirable trehalose dry powder particles in the 0.75–0.99 µm range made by the novel process of organic solution advanced spray-drying in closed-mode, as earlier reported by these authors.[49] The size and morphology of particles utilized in the inhalation application is paramount in ensuring targeted delivery to specific lung regions, since particles in the stated size range are capable of delivering a payload to a specific lung region (such as the deep lung).[17,45,50–52] While all particles that had measurable sizes were within an ideal size range, the morphology exhibited was not smooth and without agglomeration for the entire set of particles. In particular, SD particles that underwent the highest spray-drying rate of 30 mL/minute (high P systems) had the best morphology, whereas the low P and medium P systems were rough and agglomerated, which would limit the aerosolization and delivery of these particles via inhalation methods. Overall, the highest pump rate resulted in the most optimal particle set.

PXRD and DSC analysis showed that the organic solution advanced spray-drying in closed mode of dilute solutions with DPPC and/or DPPE-PEG resulted in particles that demonstrated the presence of the lipid bilayer structure (multilamellar) as evidence of the signature peaks for PXRD and the characteristic bilayer phase-transition values of T_c, T_p, and T_m, in DSC thermograms.[24–26] PXRD data were the same for both the raw and SD particles and proved the presence of both the lipid bilayer(s) and PEG within the SD systems, which were not affected by a change in pump rates. A relationship was seen between the intensity of the PXRD peaks corresponding to PEG (at 19° and 23° 2θ) and the PEG chain length, where the intensity increased with increasing PEG

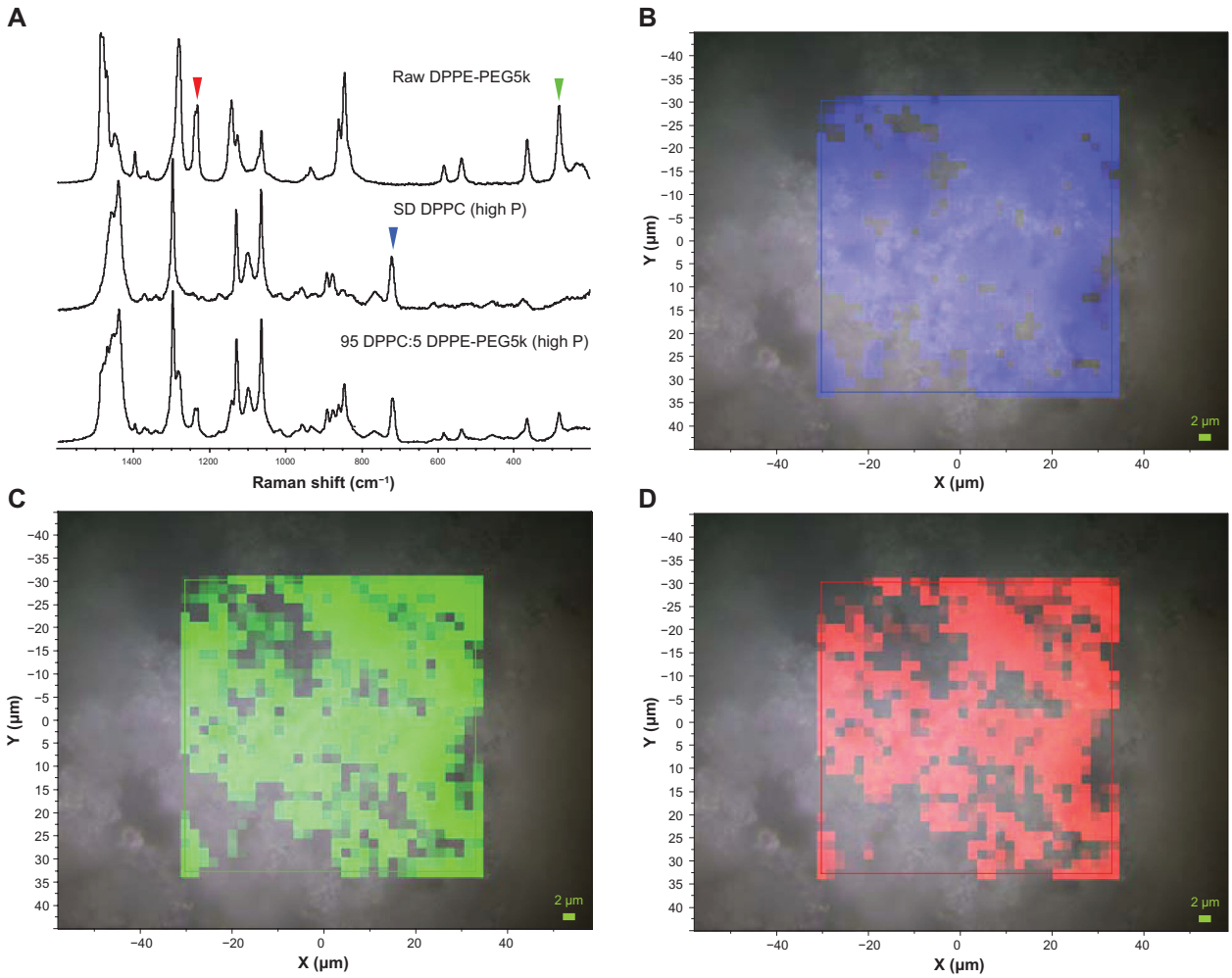

Figure 14 (**A**) Raman spectra obtained via confocal microscopy of raw dipalmitoylphosphatidylethanolamine poly(ethylene glycol)-5k (DPPE-PEG5k), formulated spray-dried (SD) dipalmitoylphosphatidylcholine (DPPC), and formulated co-SD 95 DPPC:5 DPPE-PEG5k (high P). Colored arrowheads show mapped bands. (**B**) Raman spectroscopic mapping showing the area of the Raman bands between 700 and 740 cm^{-1} (brighter colors indicate greater area) superimposed on a bright-field optical image of the surface of a particle of formulated SD DPPC (100% pump rate). (**C**) Map showing the area of the Raman bands between 270 and 295 cm^{-1}. (**D**) Map showing the area of the Raman bands between 1225 and 1250 cm^{-1}.

chain length. DSC thermograms of pure SD DPPC particles showed similar T_m values irrespective of spray-drying pump rates, which corresponded to raw DPPC without a pretransition peak. This bilayer phase transition was also present in co-SD DPPC:DPPE-PEG particles along with a secondary endothermic peak, which corresponded to that of pure raw DPPE-PEG, neither of which was dependent on the pump rate. The relationship between the endothermic peak values exhibited by the particles and the outlet temperatures from the spray-drying process was likely a significant factor in the successful formation of multilamellar particles using the fastest pump rate. The outlet temperatures for the low and medium pump rates (3 and 15 mL/minute, respectively) were above the phase-transition temperatures of the formulated PEGylated phospholipid particles, resulting in improper formation and agglomeration. A higher pump rate decreased the outlet temperature, while allowing for the formation of ideally sized, smooth particles that were not agglomerated and properties suitable for inhalation aerosol delivery as dry powders.

HSM enabled visualization as a function of temperature and confirmed the phase transitions of the raw DPPC and DPPE-PEGs, as well as the formulated SD DPPC and co-SD DPPC:DPPE-PEG SD particles. It also showed the stability of the particles at physiological temperatures. ATR-FTIR analysis on the SD particles in their dry state in comparison to their raw components confirmed the presence of both DPPC and DPPE-PEG where appropriate through the signature peaks of each of these materials without the destruction of particles that would occur using other FTIR methods. Furthermore, organic spray-drying resulted in low water content of the particles, which is necessary for effective

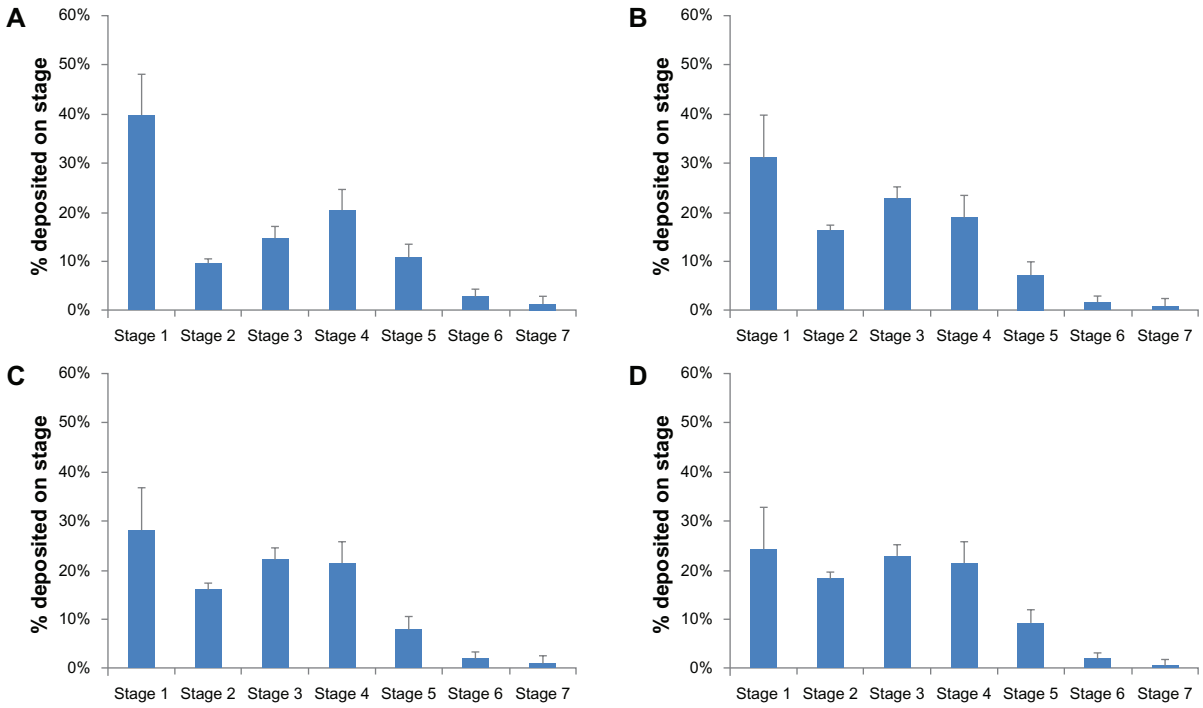

Figure 15 Aerosol-dispersion performance as % deposition on each stage of the Next Generation Impactor at Q = 60 L/minute for: (**A**) 100 dipalmitoylphosphatidylcholine (DPPC) (high P), (**B**) 95 DPPC:5 dipalmitoylphosphatidylethanolamine poly(ethylene glycol)-2k (DPPE-PEG2k) (high P), (**C**) 95 DPPC:5 DPPE-PEG3k (high P), and (**D**) 95 DPPC:5 DPPE-PEG5k (high P).
Note: High P correspond to 100% pump rate.

particle delivery since residual water can have a significant influence on impeding the dispersion of dry powder during aerosolization.[53] These values were remarkably low for inhalation applications, and this is another novel advantage in organic solution spray-drying (ie, minimizes residual water content in the final powder). Raman microscopy and chemical imaging confirmed the chemical homogeneity of the particles.

Excellent aerosol dispersion performance (Figure 15) and optimal aerosol performance parameters (Table 4) were demonstrated using the NGI™ coupled with the HandiHaler® DPI device and clearly indicated that the formulated particles would be optimal for efficient and predominant deposition into the deep lung region for targeted delivery as inhaled nanoparticles/microparticles as aerosolized powders. The MMAD values were within the range (1–5 μm) necessary for particles to deposit predominantly in the middle- to deep-lung regions and deposit by sedimentation due to gravitational settling.[1,7,8,52] For example, it was reported that porous poly(lactic-*co*-glycolic) microparticles exhibited MMADs ranging from 4.5 to 6.6 μm,[5] whereas phospholipid/mannitol SD particles ranged from 1.25 to 1.77 μm.[37] Furthermore, the ED, FPF, and RF values were all high compared to other values reported in the literature.[54,55] While not all of these

Table 4 Aerosol dispersion performance properties as aerosolized dry powders of PEGylated phospholipid particles including mass median aerodynamic diameter (MMAD), geometric standard deviation (GSD), fine particle dose (FPD), fine particle fraction (FPF), respirable fraction (RF), and emitted dose (ED) for inhalable microparticle/nanoparticle formulations all designed and produced at high P (mean ± standard deviation, n = 3)

Aerosol system	100 DPPC	95 DPPC:5 DPPE-PEG2k	95 DPPC:5 DPPE-PEG3k	95 DPPC:5 DPPE-PEG5k
MMAD (μm)	4.4 ± 0.9	4.5 ± 0.3	4.1 ± 0.2	4.0 ± 0.6
GSD (μm)	2.7 ± 0.7	2.3 ± 0.0	2.2 ± 0.3	2.1 ± 0.2
FPD (mg)	7.5 ± 1.5	9.1 ± 0.7	9.5 ± 1.1	9.0 ± 1.2
FPF (%)	23.8 ± 4.7	29.4 ± 2.8	30.2 ± 3.4	29.5 ± 4.3
RF (%)	60.3 ± 8.5	68.7 ± 5.2	71.7 ± 3.0	75.5 ± 12.8
ED (mg)	28.7 ± 1.2	29.0 ± 0.9	29.6 ± 1.2	28.6 ± 0.9
ED (%)	91.2 ± 4.0	93.1 ± 1.2	94.2 ± 2.6	93.2 ± 1.9

Abbreviations: DPPC, dipalmitoylphosphatidylcholine; DPPE, dipalmitoylphosphatidylethanolamine; PEG, poly(ethylene glycol).

aerosol performance parameters are often reported, FPF% values for porous poly(lactic-*co*-glycolic acid) particles were reported to be in the range of 10.7%–33.8%[5] and sodium alendronate from 34.4% to 62.0%.[38] The novel findings reported here indicate the significant potential of these lipopolymeric lung surfactant-mimic particles to be utilized to effectively deliver many different types of therapeutics to the lung as inhaled dry powder nanomedicine aerosols.

Conclusion

This comprehensive and systematic study demonstrated for the first time that inhalable DPPC:DPPE-PEG microparticles and nanoparticles with differing PEG lengths were rationally designed and successfully produced using the advanced organic spray-drying process in closed mode for dilute alcohol solutions. The SD lung surfactant-mimic phospholipid and lipopolymeric particles produced from various rationally chosen pump rates showed that the highest pump rate (30 mL/minute) resulted in particles with smooth, spherical morphology and optimal characteristics for inhalation aerosol delivery as DPIs. This was a result of the lower outlet temperatures exhibited, which was below the transition temperature of these particles. Pharmaceutical processing conditions correlated in a meaningful manner with changes in important physicochemical and particle properties, such as morphology and transition temperatures, essential for targeted pulmonary delivery as DPIs. These novel particles as aerosolized dry powders of lung surfactant-mimic and biocompatible lipopolymeric microparticles/nanoparticles offer the potential to be used in the delivery of a wide variety of pulmonary drugs, owing to their inherent ability to encapsulate numerous types of drugs, controlled drug release, enhanced mucus penetration by phospholipid spreading and PEG penetration, and evasion of phagocytosis by immune cells.

Acknowledgments

The authors gratefully acknowledge financial support from the National Cancer Institute (NCI) grant number R25CA153954 and a National Cancer Institute Cancer Nanotechnology Training Center (NCI-CNTC) Postdoctoral Traineeship awarded to SAM. The content is solely the responsibility of the authors and does not necessarily represent the official views of the National Cancer Institute or the National Institutes of Health. The authors thank Dr Tonglei Li for PXRD and HSM access, and Dr J Zach Hilt for ATR-FTIR access.

Disclosure

The authors report no conflicts of interest in this work.

References

1. Carvalho TC, Carbalho SR, McConville JT. Formulations for pulmonary administration of anticancer agents to treat lung malignancies. *J Aerosol Med Pulm Drug Deliv*. 2011;24:61–80.
2. Mansour HM, Rhee YS, Wu X. Nanomedicine in pulmonary delivery. *Int J Nanomedicine*. 2009;4:299–319.
3. Vaughn JM, McConville JT, Burgess D, et al. Sing dose and multiple dose studies of itraconazole nanoparticles. *Eur J Pharm Biopharm*. 2006;63:95–102.
4. Gill S, Löbenberg R, Ku T, Azarmi S, Roa WH, Prenner EJ. Nanoparticles: characteristics, mechanisms of action, and toxicity in pulmonary drug delivery – a review. *J Biomed Nanotechnol*. 2007;3:107–119.
5. Yang Y, Bajaj N, Xu P, Ohn K, Tsifansky MD, Yeo Y. Development of highly porous large PLGA microparticles for pulmonary drug delivery. *Biomaterials*. 2009;30:1947–1953.
6. Sharma S, White D, Imondi A, Placke ME, Vail DM, Kris MG. Development of inhalation agents for oncologic use. *J Clin Oncol*. 2001;19:1839–1847.
7. Hickey AJ, Mansour HM. Delivery of drugs by the pulmonary route. In: Florence AT, Siepmann J, editors. *Modern Pharmaceutics*. 5th ed. New York: Taylor and Francis; 2009;2:191–219.
8. Hickey AJ, Mansour HM. Formulation challenges of powders for the delivery of small molecular weight molecules as aerosols. In: Rathbone MJ, Hadgraft J, Roberts MS, Lane ME, editors. *Modified-Release Drug Delivery Technology*. 2nd ed. New York: Informa Healthcare; 2008;2:573–602.
9. Arnold MM, Gonnan EM, Schieber LJ, Munson EJ, Berkland C. NanoCipro encapsulation in monodisperse large porous PLGA microparticles. *J Control Release*. 2007;121:100–109.
10. Cartiera MS, Ferreira EC, Caputo C, Egan ME, Caplan MJ, Saltzman WM. Partial correction of cystic fibrosis defects with PLGA nanoparticles encapsulating curcumin. *Mol Pharm*. 2010;7:86–93.
11. Meenach SA, Kim YJ, Kauffman KJ, Kanthamneni N, Bachelder EM, Ainslie KM. Synthesis, optimization, and characterization of camptothecin-loaded acetalated dextran porous microparticles for pulmonary delivery. *Mol Pharm*. 2012;9:290–298.
12. Oh YJ, Lee J, Seo JY, et al. Preparation of budesonide-loaded porous PLGA microparticles and their therapeutic efficacy in a murine asthma model. *J Control Release*. 2011;150:56–62.
13. Wu XA, Li XJ, Mansour HM. Surface analytical techniques in solid-state particle characterization for predicting performance in dry powder inhalers. *Kona Powder Part J*. 2010;28:3–19.
14. Mansour HM, Rhee YS, Park CW, DeLuca PP. Lipid nanoparticulate drug delivery and nanomedicine. In: Moghis A, editor. *Lipids in Nanotechnology*. Urbana (IL): American Oil Chemists Society (AOCS) Press; 2011:221–268.
15. Watts AB, McConville JT, Williams RO. Advancements in dry powder delivery to the lung. *Drug Dev Ind Pharm*. 2008;34:948–959.
16. Patton JS, Byron PR. Inhaling medicines: delivering drugs to the body through the lungs. *Nat Rev Drug Discov*. 2007;6:67–74.
17. Sung JC, Pulliam BL, Edwards DA. Nanoparticles for drug delivery to the lungs. *Trends Biotechnol*. 2007;25:563–570.
18. Laube BL, Janssens HM, de Jongh FHC, et al. What the pulmonary specialist should know about inhalation therapies. *Eur Respir J*. 2011;37:1308–1331.
19. Xu Z, Mansour HM, Hickey AJ. Particle interations in dry powder inhaler unit processes. *J Adhes Sci Technol*. 2011;25:451–482.
20. Rhee YS, Mansour HM. Nanopharmaceuticals I: nanocarrier systems in drug delivery. Invited paper. *Int J Nanotechnology*. 2011;8:84–114.
21. Wu X, Mansour HM. Nanopharmaceuticals II: application of nanoparticles and nanocarrier systems in pharmaceutics and nanomedicine. Invited paper. *Int J Nanotechnology*. 2011;8:115–145.

22. Willis L, Hayes DJ, Mansour HM. Therapeutic liposomal dry powder inhalation aerosols for targeted lung delivery. *Lung*. 2012;190:251–262.
23. Ganguly S, Moolchandani V, Roche JA, et al. Phospholipid-induced in vivo particle migration to enhance pulmonary deposition. *J Aerosol Med Pulm Drug Deliv*. 2008;23:181–187.
24. Mansour HM, Zografi G. The relationship between water vapor absorption and desorption by phospholipids and bilayer phase transitions. *J Pharm Sci*. 2007;96:377–396.
25. Mansour H, Wang DS, Chen CS, Zografi G. Comparison of bilayer and monolayer properties of phospholipid systems containing dipalmitoylphosphatidylglycerol and dipalmitoylphosphatidylinositol. *Langmuir*. 2001;17:6622–6632.
26. Mansour HM, Zografi G. Relationships between equilibrium spreading pressure and phase equilibria of phospholipid bilayers and monolayers at the air-water interface. *Langmuir*. 2007;23:3809–3819.
27. Mansour HM, Damodaran S, Zografi G. Characterization of the in situ structural and interfacial properties of the cationic hydrophobic heteropolypeptide, KL_4, in lung surfactant bilayer and monolayer models at the air-water interface: implications for pulmonary surfactant delivery. *Mol Pharm*. 2008;5:681–695.
28. Mabrey S, Sturtevant JM. Investigation of phase transitions of lipids and lipid mixtures by high sensitivity differential scanning calorimetry. *Proc Natl Acad Sci U S A*. 1976;73:3862–3866.
29. Labiris NR, Dolovich MB. Pulmonary drug delivery. Part I: physiological factors affecting therapeutic effectiveness of aerosolized medications. *Br J Clin Pharmacol*. 2003;56:588–599.
30. Labiris NR, Dolovich MB. Pulmonary drug delivery. Part II: the role of inhalant delivery devices and drug formulation in therapeutic effectiveness of aerosolized medications. *Br J Clin Pharmacol*. 2003;56:600–612.
31. Ishihara K, Nomura H, Mihara T, Kurita K, Iwasaki Y, Nakabayashi N. Why do phospholipid polymers reduce protein adsorption? *J Biomed Mater Res*. 1998;39:323–330.
32. Mansour HM, Sohn M, Al-Ghananeem A, Deluca PP. Materials for pharmaceutical dosage forms: molecular pharmaceutics and controlled release drug delivery aspects. *Int J Mol Sci*. 2010;11:3298–3322.
33. Lai SK, O'Hanlon DE, Harrold S, et al. Rapid transport of large polymeric nanoparticles in fresh undiluted human mucus. *Proc Natl Acad Sci U S A*. 2007;104:1482–1487.
34. Sadikot RT, Rubinstein I. Long-acting, multi-targeted nanomedicine: addressing unmet medical need in acute lung injury. *J Biomed Nanotechnol*. 2009;5:614–619.
35. Lim SB, Rubinstein I, Sadikot RT, Artwohl JE, Önyüksel H. A novel peptide nanomedicine against acute lung injury: GLP-1 in phospholipid micelles. *Pharm Res*. 2011;28:662–672.
36. Kikuchi H, Yamauchi H, Hirota S. A spray-drying method for mass production of liposomes. *Chem Pharm Bull*. 1991;36:1522–1527.
37. Alves GP, Santana MHA. Phospholipid dry powders produced by spray drying processing: structural, thermodynamic and physical properties. *Powder Technol*. 2004;145:139–148.
38. Cruz L, Fattal E, Tasso L, et al. Formulation and in vivo evaluation of sodium alendronate spray-dried microparticles intended for lung delivery. *J Control Release*. 2011;152:370–375.
39. Bosquillon C, Lombry C, Preat V, Vanbever R. Influence of formulation excipients and physical characterisitcs of inhalation dry powders on their aerosolization performance. *J Control Release*. 2001;70:329–339.
40. Bi R, Shao W, Wang Q, Zhang N. Spray-freeze-dried dry powder inhalation of insulin-loaded liposomes for enhanced pulmonary delivery. *J Drug Target*. 2008;16:639–648.
41. Masters K. *Spray Drying Handbook*. 5th ed. Harlow, UK: Longman; 1991.
42. Li X, Mansour HM. Physicochemical characterization and water vapor absorption of organic solution advanced spray dried trehalose microparticles and nanoparticles for targeted dry powder pulmonary inhalation delivery. *AAPS Pharm Sci Tech*. 2011;12:1420–1430.
43. Park CW, Rhee YS, Vogt F, et al. Advances in microscopy and complementary imaging techniques to assess the fate of drugs ex-vivo in respiratory drug delivery: an invited paper. *Adv Drug Deliv Rev*. 2012;64:344–356.
44. Chapter 601. Aerosols, nasal sprays, metered-dose inhalers, and dry powder inhalers monograph. In: *USP 29-NF 24: United States Pharmacopoeia and the National Formulary: The Official Compendia of Standards*. Vol 29/24. Rockville, MD: United States Pharmacopeial Convention; 2006:2617–2636.
45. Edwards DA, Ben-Jebria A, Langer R. Recent advances in pulmonary drug delivery using large, porous inhaled particles. *J Appl Physiol*. 1998;85:379–385.
46. Kang E, Robinson J, Park K, Cheng JX. Paclitaxel distribution in poly(ethylene glycol)/poly(lactide-co-glycolic acid) blends and its release visualized by coherent anti-Stokes Raman scattering microscopy. *J Control Release*. 2007;122:261–268.
47. Jones BG, Dickinson PA, Gumbleton M, Kellaway IW. The inhibition of phagocytosis of respirable microspheres by alveolar and peritoneal macrophages. *Int J Pharm*. 2002;236:65–79.
48. Wu YP, Zuo F, Zheng ZH, Ding XB, Peng YX. A novel approach to molecular recognition surface of magnetic nanoparticles based on host-guest effect. *Nanoscale Res Lett*. 2009;4:738–747.
49. Li X, Hayes D, Mansour HM. Targeted lung delivery by inhalable multifunctional microparticulate/nanoparticulate aerosols for cystic fibrosis combination drug/mucolytic treatment. *Pediatric Pulmonology*. 2011:34 Suppl:346.
50. Azarmi S, Roa WH, Lobenberg R. Targeted delivery of nanoparticles for the treatment of lung diseases. *Adv Drug Deliv Rev*. 2008;60:863–875.
51. Gautam A. Targeted delivery of therapeutics by aerosol for cancer of the lung. *Curr Cancer Drug Targets*. 2003;3:57.
52. Edwards DA. The macrotransport of aerosol particles in the lung: aerosol deposition phenomena. *J Aerosol Sci*. 1995;26:293–317.
53. Hickey AJ, Mansour HM, Telko MT, et al. Physical characterization of component particles included in dry powder inhalers. I. Strategy review and static characteristics. *J Pharm Sci*. 2007;96:1282–1301.
54. Vanbever R, Ben-Jebria A, Mintzes J, Langer C, Edwards DA. Sustained release of insulin from insoluble inhaled particles. *Drug Dev Res*. 1999;48:178–185.
55. Ungaro F, De Rosa G, Miro A, Quaglia F, La Rotonda MI. Cyclodextrins in the production of large porous particles: development of dry powders for the sustained release of insulin to the lungs. *Eur J Pharm Sci*. 2006;28:423–432.